ASEG-PESA 2015
Geophysics and Geology together for Discovery
24th International Geophysical Conference and Exhibition
15–18 February 2015 Perth, Western Australia

Application of seismic attributes for constraining Magnetotelluric Inversion

Cuong Van Anh Le
DET CRC, Curtin University
ARRC/CSIRO Building, H Block, Level 4, 26 Dick Perry Avenue, Kensington
v.le3@postgrad.curtin.edu.au

Brett Harris
DET CRC, Curtin University
ARRC/CSIRO Building, H Block, Level 4, 26 Dick Perry Avenue, Kensington
B.Harris@curtin.edu.au

Eric Takam Takougang
DET CRC, Curtin University
ARRC/CSIRO Building, H Block, Level 4, 26 Dick Perry Avenue, Kensington
eric.takam@curtin.edu.au

Andrew Pethick
DET CRC, Curtin University
ARRC/CSIRO Building, H Block, Level 4, 26 Dick Perry Avenue, Kensington
andrew.pethick@curtin.edu.au

SUMMARY

Unconstrained inversion of surface magnetotelluric data generates non-uniqueness solutions. Boundaries derived from seismic reflectively images have the potential to substantially improve MT inversion. Seismic should be highly beneficial where significant and strong reflectors can reasonably be associated with contrast in electrical conductivity across well-defined relatively continuous boundaries. We show how seismic reflections can assist in defining such inversion controls as the smoothness penalty across known boundaries. We apply and compare a range of cooperative inversion strategies using large scale co-located magnetotelluric and seismic reflection field data sets from the Carlin style gold district in Nevada USA.

Key words: Magnetotelluric, inversion, covariance, conductivity.

INTRODUCTION

Magnetotelluric (MT) inversion using constraints derived from seismic data can potentially improve subsurface imaging. MT can recover subsurface conductivity distribution. Resolution rapidly decreases with depth because high frequency electromagnetic fields are strongly attenuated, leaving only low frequency electromagnetic fields. These low frequency fields tend to be very poor at resolving deep sharp boundaries. In reality sharp layers and conductive anomalies may appear after inversion as highly smoothed transitions or smeared 'blobs' respectively. Unwanted artefacts masquerading as true anomalies are also frequently found within inversion outcomes. Seismic reflection methods do not suffer the same loss of resolution with depth. In one example from the Red Sea area (Colombo et al., 2013) interpretation into MT inversion results were substantially valid when boundaries interpreted from migrated seismic sections show correlation to the MT resistivity distribution and MT results support seismic velocity building of areas in which the seismic data could not work well. Joint inversion using the cross gradient approach can improve the definition of structural features by minimizing the variation of the cross gradient of two or more earth properties such as velocity and conductivity (Gallardo and Meju, 2004) provided that the earth properties are structurally linked (i.e. change in the same direction).

Prior boundary information derived from seismic reflection data may provide a valuable constraint on MT inversion if the "precise" locations of geological structures such as layers and faults can be recovered. In this paper, we present smooth MT inversion combined with representation of sharp seismic boundaries. These boundaries information are converted into smoothness penalty matrix to force MT inversion.

METHOD AND RESULTS

The Smooth approach is commonly used to invert MT data to predict subsurface electrical resistivity distributions. For example, the Smooth Occam objective function (deGroot-Hedlin and Constable, 1990) is shown in equation (1) . The Smooth Occam algorithm has two main requirements, (i) satisfying misfit of field and synthetic data and (ii) setting the similarity level of resistivity in adjacent positions.

$$U[m] = \left\|\partial_y m\right\|^2 + \|\partial_z m\|^2 + \mu^{-1}\{\|Wd - WF(m)\|^2 - X_*^2\}, \quad (1)$$

where $\left\|\partial_y m\right\|^2 + \|\partial_z m\|^2$ is a roughening matrix which expresses differences of the model parameters for laterally or vertically adjacent cells. Here μ^{-1} is the Lagrange multiplier and U[m] is the objective function. W is the weighting matrix expressing the data error, d data, m the model parameter, F a forward modelling operator, and X_* is target misfit. Minimization of the objective function is to recover the resistivity model. The Lagrange multiplier plays a key role in balancing the two main requirements.

It is difficult to invert to a sharp boundary with the conventional smooth approach. However, deGroot-Hedlin and Constable (1990) demonstrate how the addition of a sharp boundary from prior information, such as seismic boundaries, can be included within Occam inversion. They show that the penalty for roughening at the boundary could be avoided by inserting zeroes at positions inside the roughening matrix corresponding to the defined seismic boundary. This approach can then force a sharp boundary but retain smoothness in the volume on each side of the boundary.

Results

2D synthetic data

The model (Figure 1) consists of two square blocks within a uniform halfspace. The left conductive block is 5 Ω·m and the right resistive block is 2000 Ω·m. The background half-space resistivity is 100 Ω·m. This model is the same as presented by deGroot-Hedlin and Constable (1990) in their analysis of Occam inversion.

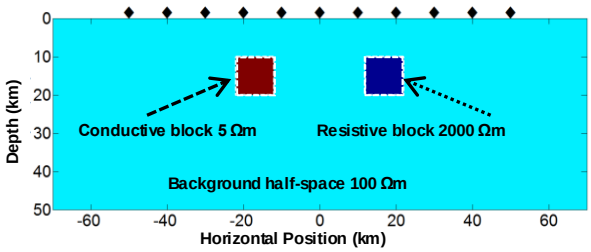

Figure 1: The 2D geo-electrical synthetic model used for testing the MT inversion code. The dashed white lines express the boundaries of the two square blocks, conductive and resistive. The diamond shapes represent the station positions. The model is the same as used by deGroot-Hedlin and Constable (1990).

We invert synthetic surface MT data generated over this model for three inversion scenarios, which are: (i) inversion without boundary, (ii) Sharp Inversion with correctly defined boundaries for the two blocks, and (iii) Sharp Inversion with incorrect, oversized block boundaries (see Figure 2c). The background starting model is a 1 Ω·m homogeneous half-space for all three inversion scenarios. The examples demonstrate the three inversions:

i. Smooth Occam inversion with no boundary information forces smooth transition between earth model cells in every location throughout the full model domain and for an earth with sharp boundaries. This produces artifacts within the background or host rock (i.e., conductive and resistive shadows).
ii. Occam inversion with perfectly located boundaries has accurate recovered the resistivity of both blocks (i.e., approximately 600 Ω·m and 4 Ω·m for resistive and conductive blocks respectively) and shows reduced presence of artifacts in the surrounding half-space.
iii. Sharp Inversion with incorrectly located boundaries has also resulted in a reasonable estimate of conductivity and locations of the two blocks. The key outcome here is that there is a significant reduction in the artifacts generated outside the two blocks in particular at depth.

It appears that the resistive block does not have any effect on the residual percentage in each of the inversion cases. In the inversion scheme using the correct boundary information, a substantial decrease in the residual percentage is evident in the region of the higher frequencies (Figure 2e) whose presence can be explained by the attenuation of higher frequencies (e.g., skin depth equation).

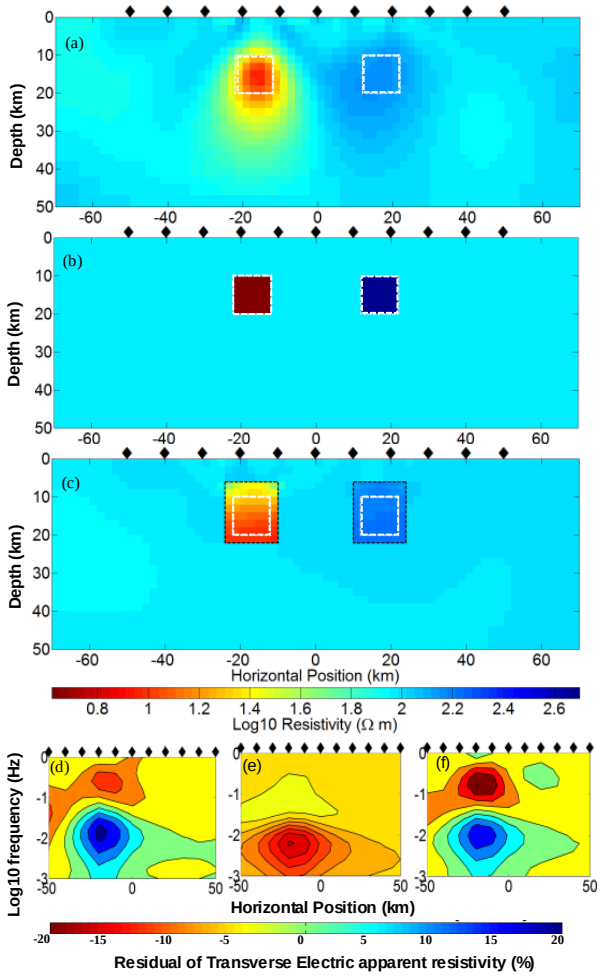

Figure 2: The 2D MT data inversion results (i.e., conductivity distributions and percentage residuals of transverse electric (TE) apparent resistivity) for the two block models presented in Figure 1. Figure 2a shows the resistivity distribution resulting from smooth Occam inversion without boundary constraints (this is similar to the result shown by deGroot-Hedlin and Constable (1990)). Figure 2b is the resistivity distribution resulting from Occam inversion that includes explicit and accurate model boundary conditions at four edges of the two blocks. Figure 2c is the resistivity distribution derived from Occam inversion where incorrect boundary definition constrains the inversion. The black dotted squares are the boundaries used for inversion and the white dotted squares show the edges of the two blocks for the actual model. Figures 2d, 2e, and 2f express percentage residuals between the synthetic MT TE mode apparent resistivity and inverted TE mode apparent resistivity for the three cases: (i) no priori boundary information (Figure 2d), (ii) inclusion of correct boundary information (Figure 2e), and (iii) inclusion of wrong boundary information (Figure 2f), respectively.

Field data

We apply the previously stated approach to invert MT data from a location in the Carlin style gold district in Nevada, USA. The data consists of a seismic line co-located with MT data. We used MT field data recorded with 18 stations, each with an MT measurement containing 51 frequencies ranging

from 0.1 to 640 Hertz. We have chosen all initial models to be isotropic with all cells set to 100 Ω·m.

Figure 3 shows a 2D seismic section extracted from a 3D seismic volume along the MT transect. Features to note in Figure 3 are: (i) the normal fault (black dashed line) and (ii) the high reflectivity interface between shallow, relatively conductive, low velocity sediments and more electrically resistive, higher velocity "basement rock" (i.e., the white dotted line).

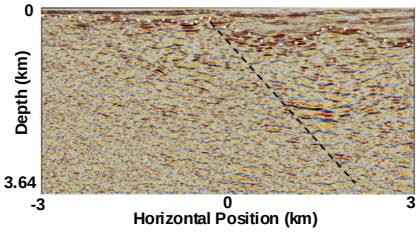

Figure 3: Seismic section collocated with MT measurement line. The white points indicate a seismic boundary. Dash black line represents the fault trend.

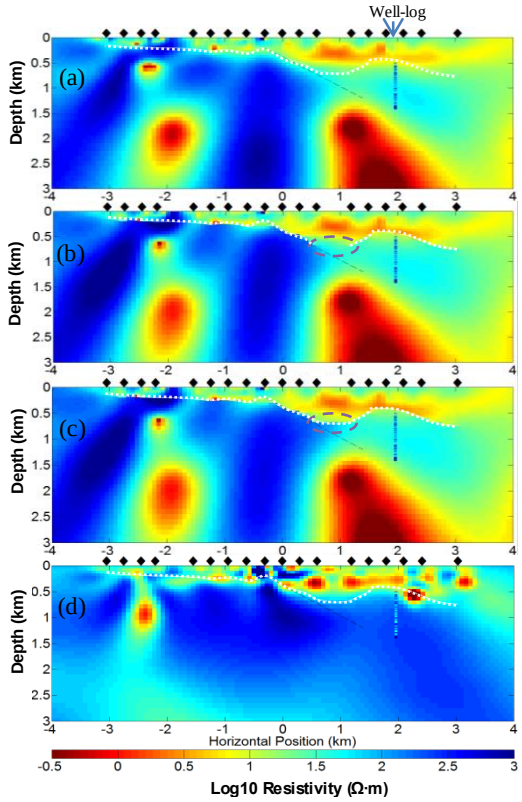

Figure 4: MT inversion resistivity recovered using the Occam program (deGroot-Hedlin and Constable, 1990) and modEM2D program (Egbert and Kelbert, 2012): (a) Occam inversion without additional seismic boundary, (b) Occam inversion with discontinuous boundary, (c) Occam inversion with continuous boundary, and (d) modEM2D inversion without additional seismic boundary. The dashed white lines represent boundary information mentioned in MT inversion. There are large differences in resistivity distribution between MT results of Occam and modEM2D. Two large, smoothly varying conductive features located around depth 2km are not present in the modEM2D result. The resistivity background below the boundary line (the white dotted line) in the modEM2D result is higher than in the Occam results.

We use Occam inversion (i.e. OCCAM2D) (deGroot-Hedlin and Constable, 1990) and that described by Egbert and Kelbert (2012) (i.e., modEM2D) to invert the MT data into conductivity distributions. Occam inversion (see Figures 4a, 4b, and 4c) uses Finite Element forward modelling and Cholesky factorization as core elements of the inversion algorithm, while modEM2D (used in Figure 4d) uses a Finite Difference solver for forward modelling and the Non-linear Conjugate Gradient method within the inversion.

Figure 4 shows the conductivity distribution derived from four inversion workflows. We note again that all inversion commences with a 100 Ω·m half-space model. The four MT inversion cases are presented as in Figure 4 are:

i. unconstrained Occam inversion (Figure 4a),
ii. incomplete boundary constrained Occam inversion with the key high reflectivity boundary included (Figure 4b). The omitted boundary constraint found in previous models is marked as a purple dotted oval shape. We deliberately excluded this length of the high reflectivity boundary (see Figure 4c for comparison with a complete boundary),
iii. boundary constrained Occam inversion with the high reflectivity continuous boundary interpreted from the seismic (Figure 4c), and
iv. unconstrained inversion using the ModEM2D approach of Egbert and Kelbert (2012) (Figure 4d).

Note that a wireline log of resistivity was acquired from the base of shallow sediments (~500m) to a depth of approximately 1500m below ground level. The resistivity log is provided for reference as shown in Figures 4a, 4b, 4c, and 4d.

The key points from the field example presented in Figure 4 are:

i. The Smooth Occam inversion, as is commonly used in industry, is likely to generate artifacts at depth below a shallow conductive zone (Figure 4a). It is geologically reasonable that sharp electrically resistive boundaries exist in this setting. However, artefacts occurred when existing sharp boundaries are not accommodated in the inversion. This inferred result supports the findings from our synthetic examples (see Figure 2a).
ii. The inversion used to derived Figure 4b retained the sharp boundary at the high reflectivity interface except in the zone indicated by the purple dotted oval. A smooth and probably artificial transition zone where geologically it should likely be sharp exists.
iii. Occam Inversion, inclusive of a sharp continuous boundary, has resulted in a sharp transition at the high reflectivity boundary. However, because the inversion is compelled to smoothly vary the conductivities external to this boundary, Figures 4a, 4b, and 4c show much greater similarities in these unconstrained regions. The deep conductivity looks similar and may not represent the true geo-electrical distribution and may change if a complete interpretation of sharp boundary distributions from the seismic image is used to constrain the model. This also requires a greater detailed interpretation of the subsurface in addition to the application of seismic and electrical property relationships. Only one well for calibration could be obtained and therefore have not pursued these complex interpretations which may require multiple boundaries to be included in the MT inversion.
iv. The inversion algorithm itself plays a highly significant role in the outcome. The modEM2D inversion facilitates greater focusing of high conductivity zones in the shallower more conductive and more rapidly changing

sediments. The result appears to be that the deeper conductivity anomalies have "disappeared". It may be that the shallow conductivity distribution is better accommodated by the modEM2D (Egbert and Kelbert, 2012). However, we also found that the criteria used for fitting errors tend to create or move different conductive zones below the shallow sediments.

Much care is required when using any form of cooperative or joint inversion of seismic and MT data. There are several circumstances where imposing structural or boundary constraints may lead to a result worse than independent inversion. Four examples are provided below.

i. Anisotropy: The upper younger cover sequences at this site exhibit classic sub-horizontal laying and we would strongly suspect electrical transverse isotropy. For low energy sequences (shale and siltstone) vertical to horizontal resistivity could be more than 1:10. Where these sub-horizontal electrically anisotropic sediments are truncated by large sub-vertical fault systems, the impact of unaccounted for anisotropy could be significant.
ii. Three dimensional effects: The modelling was completed with 2D inversion. This is a reasonable approximation; however, when depth increases and the dominant frequency decreases the impact of 3D effects becomes more severe and can be expressed as artefacts.
iii. Solute distribution in shallow sediments: Basin hydrodynamics must always be considered. That is the distribution of dissolved salts in the saturated cover sediments may not be linked in simply way to sedimentary layering.
iv. High angle Faults: Faults can form narrow and relatively electrically conductive zones in an otherwise electrically resistive background. This is particularly the case if pressure and temperature associated with faulting or reactivation has resulted development of clayey minerals in the fault zone or if there is saline water in open fractures. Recovery of these narrow sub-vertical high conductivity zones are challenging for both seismic processing/inversion and MT inversion.

Better strategies for building the above factors into seismically constrained MT inversion need to be developed.

CONCLUSIONS

We have provided synthetic and field examples demonstrating how seismic information can potentially improve MT results where the start model for all inversions was a common homogeneous half-space. We note that in circumstances where the wrong information is entered as a constraint, the outcome may be "worse" than independent unconstrained smooth model inversion. Creating and retaining a clear record of the MT inversion workflow used to create each MT derived conductivity distribution is essential.

ACKNOWLEDGMENTS

The work has been supported by the Deep Exploration Technologies Cooperative Research Centre whose activities are funded by the Australian Government's Cooperative Research Centre Programme. This is DET CRC Document 2014/546. We also acknowledge and thank Barrick Gold Corporation for use of their comprehensive geophysical datasets.

REFERENCES

Colombo, D., G. McNeice, E. Curiel, and A. Fox, 2013, Full tensor CSEM and MT for subsalt structural imaging in the Red Sea: Implications for seismic and electromagnetic integration: The Leading Edge, 32, 436-449.

deGroot-Hedlin, C., and S. Constable, 1990, Occam's inversion to generate smooth, two-dimensional models from magnetotelluric data: Geophysics, 55, 1613-1624.

Egbert, G. D., and A. Kelbert, 2012, Computational recipes for electromagnetic inverse problems: Geophysical Journal International, 189, 251-267.

Gallardo, L. A., and M. A. Meju, 2004, Joint two-dimensional DC resistivity and seismic travel time inversion with cross-gradients constraints: Journal of Geophysical Research: Solid Earth, 109, B03311.

Last, B., and K. Kubik, 1983, Compact gravity inversion: Geophysics, 48, 713-721.

Raiche, A., 1994, Modelling and inversion -progress, problems, and challenges: Surveys in Geophysics, 15, 159-207.

Siripunvaraporn, W., and G. Egbert, 2009, WSINV3DMT: Vertical magnetic field transfer function inversion and parallel implementation: Physics of the Earth and Planetary Interiors, 173, 317-329.

Xiang, Y., P. Yu, X. Zhang, R. Tang, and C. Zhao, 2013, MT regularized inversion based on the minimum support gradient stabilizing functional, SEG Technical Program Expanded Abstracts 2013, 830-834.

Zhdanov, M. S., 2009, New advances in regularized inversion of gravity and electromagnetic data: Geophysical Prospecting, 57, 463-478.